Ventral and Dorsal Stream Interactions during the Perception of the Müller-Lyer Illusion: Evidence Derived from fMRI and Dynamic Causal Modeling

Thorsten Plewan[1], Ralph Weidner[1], Simon B. Eickhoff[1,2], and Gereon R. Fink[1,3]

Abstract

■ The human visual system converts identically sized retinal stimuli into different-sized perceptions. For instance, the Müller-Lyer illusion alters the perceived length of a line via arrows attached to its end. The strength of this illusion can be expressed as the difference between physical and perceived line length. Accordingly, illusion strength reflects how strong a representation is transformed along its way from a retinal image up to a conscious percept. In this study, we investigated changes of effective connectivity between brain areas supporting these transformation processes to further elucidate the neural underpinnings of optical illusions. The strength of the Müller-Lyer illusion was parametrically modulated while participants performed either a spatial or a luminance task. Lateral occipital cortex and right superior parietal cortex were found to be associated with illusion strength. Dynamic causal modeling was employed to investigate putative interactions between ventral and dorsal visual streams. Bayesian model selection indicated that a model that involved bidirectional connections between dorsal and ventral stream areas most accurately accounted for the underlying network dynamics. Connections within this network were partially modulated by illusion strength. The data further suggest that the two areas subserve differential roles: Whereas lateral occipital cortex seems to be directly related to size transformation processes, activation in right superior parietal cortex may reflect subsequent levels of processing, including task-related supervisory functions. Furthermore, the data demonstrate that the observer's top–down settings modulate the interactions between lateral occipital and superior parietal regions and thereby influence the effect of illusion strength. ■

INTRODUCTION

Visual illusions demonstrate that contextual information affects perception. For example, the Müller-Lyer illusion (Müller-Lyer, 1889) alters the perceived length of a line via arrows attached to its ends that either point inward or outward. Apparently, two identical retinal stimuli are transformed into different-sized representations, generating different size perceptions. The difference between retinal and perceived size is defined as the strength of the illusion. It indicates the amount of transformation a stimulus representation undergoes while being processed to a level where it influences behavior. In the case of the Müller-Lyer illusion, this strength depends on the arrows' lengths and the angle enclosed (Pressey & Martin, 1990; Erlebacher & Sekuler, 1969).

Interestingly, this alteration of perceived size has a relatively weaker effect on visually guided action than conscious report (e.g., Bruno & Franz, 2009). This has been taken as evidence that the visual system may contain two separable (albeit interacting) units. According to this explanation, originally postulated by Milner and Goodale (1995), "vision for perception" involves the ventral visual stream, whereas "vision for action" involves brain areas located within the dorsal visual stream.

Consistent with this idea, it has been demonstrated that brain areas within the ventral visual pathway are, indeed, closely associated with illusion processing. For instance, the lateral occipital cortex (LOC) contributes to a variety of visual illusions such as illusory contours or optical geometric illusions (Weidner, Boers, Mathiak, Dammers, & Fink, 2010; Weidner & Fink, 2007; Brighina et al., 2003; Ritzl et al., 2003; Seghier et al., 2000; Hirsch et al., 1995).

Findings are less conclusive with regard to the dorsal visual stream. On the one hand, the dorsal pathway is not blind to illusory information (Bruno & Franz, 2009; Bruno, Bernardis, & Gentilucci, 2008). For example, a study investigating the neural mechanisms underlying the Müller-Lyer illusion confirmed the role of ventral visual areas in illusion processing but also demonstrated that illusion strength modulates neural activity in the dorsal visual stream, namely in the right superior parietal cortex (SPC; Weidner & Fink, 2007).

[1]Research Centre Jülich, [2]Heinrich-Heine University, Düsseldorf, Germany, [3]Cologne University

On the other hand, studies involving brain-damaged patients pointed out that extrastriate areas seem to have a more prominent role in illusion processing than SPC (Vallar & Daini, 2006; Daini, Angelelli, Antonucci, Cappa, & Vallar, 2002). Subsequently, in a recent study with healthy volunteers, the functional relevance of SPC in the processing of visual illusions was tested by TMS. Whereas TMS over LOC significantly decreased the strength of the Müller-Lyer illusion, TMS over right SPC resulted only in a numerical (nonsignificant) decrease of illusion strength (Mancini, Bolognini, Bricolo, & Vallar, 2011). On the basis of this observation, it was concluded that SPC may not be involved in generating the illusion per se. In other words, the right SPC could be considered as a higher level processing unit receiving information from LOC rather than interactively contributing to the transformation from retinal to perceived size. If that conclusion is correct, illusion related activation in LOC is expected to causally affect processing in SPC but not vice versa. This hypothesis is directly amenable to testing by investigating effective connectivity between ventral and dorsal stream areas during illusion perception, using fMRI and dynamic causal modeling (DCM; Friston, Harrison, & Penny, 2003). Moreover, to dissociate different levels of processing, we tested whether signal changes as well as the underlying neural dynamics were modulated by endogenous cognitive settings. Accordingly, healthy volunteers performed either a spatial task, that is, the perceptual landmark task (Fink et al., 2000; Bisiach, Ricci, Lualdi, & Colombo, 1998), or alternatively a luminance task.

In the landmark task, participants indicated whether stimuli were correctly prebisected or not. In the luminance task, the same stimuli were judged with regard to luminance aspects of the stimulus. The stimuli used consisted of an adaptation of the Brentano version of the Müller-Lyer illusion. During both tasks, illusion strength was modulated by varying the angles of the illusion-inducing arrows.

On the basis of previous findings (Weidner et al., 2010; Weidner & Fink, 2007), we hypothesized that illusion strength is coded in both ventral and dorsal stream areas. Furthermore, we expected the connectivity analysis to unveil the interactions between these areas, that is, whether ventral stream areas drive activations in the dorsal stream or vice versa. In addition, we presumed that the spatial top–down context as induced by the landmark task modulates processing within this network. In particular, we expected that spatial top–down context would alter higher (postattentive) aspects of illusion coding, whereas early (preattentive) levels of representation would remain unaffected by top–down settings.

METHODS

Participants

Twenty-four healthy participants (nine women) participated in a single fMRI experiment. Participants were paid for their participation and gave informed consent before the experiment in accordance with the Declaration of Helsinki. The study was approved by the ethics committee of the German Society of Psychology. Participants' ages ranged from 21 to 39 years (median = 26 years). All participants had a normal or corrected-to-normal vision.

Stimuli

Stimuli were displayed on a shielded LCD monitor mounted outside the scanner on the wall behind the subject's head. The screen was seen via a mirror system mounted on top of the head coil. There were four possible stimulus positions, which were located diagonally around the center of the screen. Thus, the stimulus center and the screen center were about 1.9° visual angle apart. Locations were allocated randomly with the exception that the location was never identical in two consecutive trials.

The stimuli in the present experiment consisted of a horizontal line (about 4.4° visual angle) with an arrow-like element (approximately 0.9° visual angle) at each end and a third arrow-like element bisecting the horizontal line into two segments. All of these elements were bounded by either a circle or a diamond (Figure 1). The arrow-like elements were arranged in such a way that they formed a variant of the Müller-Lyer illusion, where one segment of the line is perceptually enlarged, whereas the other segment is perceptually diminished (Figure 1).

Across trials, the stimuli were independently varied with regard to three aspects: (1) the angle between the arrows' fins, (2) the position at which the horizontal line was bisected, and (3) the luminance of the bounding objects (i.e., the circle or the diamond).

Angles

It is known that the illusion strength generated by Müller-Lyer figures depends on the angle enclosed by its arrows (Pressey & Martin, 1990; Erlebacher & Sekuler, 1969). Thus, the perceived position at which a horizontal line is bisected is affected by the angles enclosed by the arrows (and thus by illusion strength). For instance, with an angle of 180° (Figure 1, left) no illusion is induced. Accordingly, a vertical line that bisects the horizontal line at its physical midpoint is exactly perceived in the middle. Changing the angles between the arrows' fins shifts the perceived midpoint away from the actual physical midpoint. Thereby, smaller angles increase this perceived shift. Similarly, a vertical line that bisects the horizontal line at a location that is physically displaced from the objective midpoint (e.g., by 10% of the overall length of the horizontal line) is only perceived exactly at this location when no illusion is induced (i.e., with an 180° angle between the fins of the arrow). Again, altering the arrow's angles will shift the perceived position away from this location. Using the appropriate angle configuration, the perceived position can be moved in such a way that it appears to bisect the horizontal line right in the middle. Thus, illusion strength

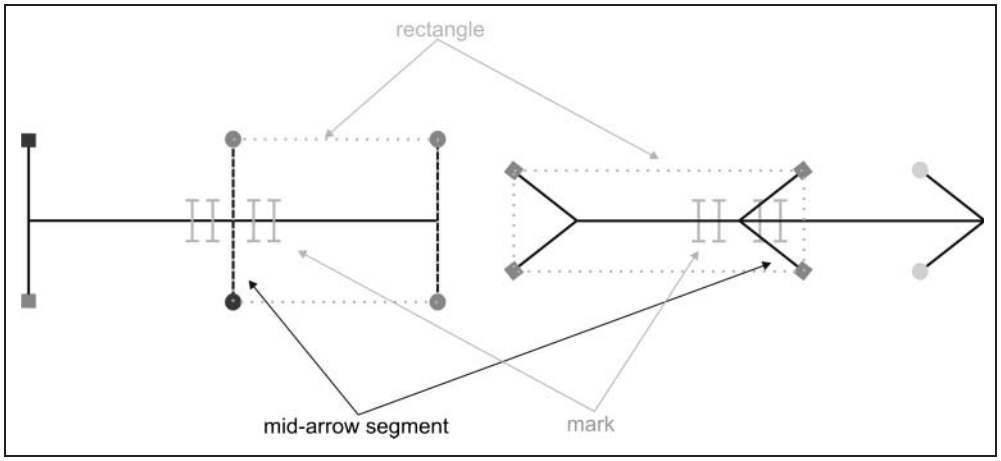

Figure 1. Examples of (Müller-Lyer) figures used in the fMRI experiment. On the left, the neutral figure is shown, which is physically correctly prebisected. The four marks indicate the other possible locations of the midarrow segment (shifted either 5% or 10% to the left or right, respectively). On the right, the perceived center is shifted to the left (via modulation of the wings' angles) and corresponds to the leftmost mark in the neutral figure. As in the left part of the figure, the (light gray) marks represent the four other possible positions of the midarrow segment (the most right mark resides on the physical middle of the horizontal line). In the landmark task participants had to indicate whether the midarrow segment bisects the horizontal line correct or not. Also the two parts of the figure show two possible configurations of the bounding objects. In the right figure, a "rectangle" is constituted with all four elements having the same luminance, whereas in the left figure, there is a diverging element within the "rectangle." In the luminance task, the participants were asked to decide whether there was a deviating element within the "rectangle" or not. The dotted lines in the figure serve to elucidate the "rectangle" and were not shown during the experiment.

compensates the actual physical displacement (i.e., the perceived shift equals 10% of the overall length of the horizontal line).

The strength of the illusion was individually adjusted across subjects to account for interindividual variability concerning the susceptibility to illusions (Hamburger & Hansen, 2010). The latter was achieved as follows: Before the fMRI measurement, participants, while already lying in the scanner, saw the illusion-inducing stimuli (as illustrated in Figure 1) and were asked to alter the angles between the arrows (by button-press) to adjust the strength of the illusion. The aim of this procedure was to identify angle configurations that induce perceptual shifts that equal 10% or 20% of the overall length of the horizontal line (see below). For this purpose, the horizontal line was kept constant across trials, and the midarrow segment was shifted 5% or 10% to the left or right side relative to the physical midpoint (see Figure 1). Participants were instructed to adjust the arrows in such a way that both segments of the prebisected line were perceived as equally long (i.e., that the horizontal line appears to be bisected in the middle). Thus, the perceived length of the two line segments was identical, albeit one segment physically occupied 10% or 20% more of the (constant) overall length (see Figure 1). During this prescanning procedure, each adjustment was repeated four times for each of the four line configurations in a randomized order.

This procedure ensured individually matched illusion strengths of 10% or 20% across subjects (henceforth, "10% illusion" and "20% illusion") for both the leftward and rightward pointing Müller-Lyer figure (henceforth, "-left" and "-right"). These four angle values were used during the main exeriment. In addition, there was a neutral condition where the arrow's fins were fixed to an 180° angle (i.e., vertical lines).

Position of Bisection

The Müller-Lyer figures presented during the main experiment involved different bisection positions. For each angle configuration derived during the prescanning procedure, there were five different positions where the midarrow segment could bisect the horizontal line (see Figure 1): One of these positions was located on the position of subjective equality, that is, the participant perceived the arrow exactly at the middle of the horizontal line. Alternatively, the midarrow segment was shifted either 5% or 10% (relative to the absolute line length) to the left or right of the position of subjective equality.

For instance, in the 10% illusion-right condition, the possible positions ranged from 20% to the left up to the physical center of the line, as indicated in Figure 1 (right). To make it more clear, in this condition, the perceived center was shifted 10% to the left relative to the physical center. Consequently, the positions of bisection were centered around this point with possible shifts of 5% or 10% to either side.

The order of conditions as well as the position of the bisection were independendly randomized and counterbalanced across the experiment.

Luminance of the Bounding Objects

All arrows had objects attached to the wings' ends (Figure 1). Each illusion figure hence comprised the line, the three arrows and six objects, four of which were of the same shape (i.e., four circles and two squares or alternatively four squares and two circles).

The four identical objects always constituted an imaginary rectangle, which was either located on the left or right side of the Müller-Lyer figure (see dotted lines in

Figure 1). The objects were presented in a medium gray (62.70 cd/m^2). However, each illusion figure contained two objects that differed in brightness and were presented in a lighter (83.45 or 104.70 cd/m^2) or darker gray (7.59 or 38.42 cd/m^2).

Task and Design

Stimuli were presented in blocks of five trials (2-sec duration each). Trials were separated by an intertrial interval. Between each trial, the interval's duration was randomly set to 2, 2.25, 2.5, 2.75, or 3 sec. Before each block, a semantic cue was presented for 1.5 sec informing the participants whether the landmark task (instruction: length) or the luminance task (instruction: form) had to be performed. Alternatively, participants were informed that a blank screen (instruction: break) would be presented. A total of 24 blocks of each condition (landmark task, luminance task) were presented in a randomized order, separated by baseline (break) periods. Each block lasted 24 sec. Thus, the overall experimental time was about 29 min.

In the landmark task, participants indicated by a right-hand button press whether they perceived the horizontal line as correctly prebisected (index finger) or not (middle finger). In the luminance task, participants indicated whether all of the four identically shaped elements were of the same luminance (index finger) or not (middle finger). In the baseline condition, the instruction was followed by a blank screen for the duration of a normal block with no task requirements.

fMRI Measurement

Functional imaging data were acquired by means of a 3-T TRIO MRI system (Siemens, Erlangen, Germany) using a T2*-weighted EPI sequence (repetition time = 2.2 sec, echo time = 30 msec). A total of 800 volumes were acquired. Each volume consisted of 36 axial slices (thickness = 3 mm, distance factor = 10%, field of view = 200 mm, 64 × 64 matrix, in-plane voxel size = 3 × 3 mm^2). Images were first spatially realigned to correct for interscan movement. Then, the mean EPI image for each participant was computed and spatially normalized to the Montreal Neurological Institute template using the "unified segmentation" function in SPM8 (Ashburner & Friston, 2005). The data were then smoothed using a Gaussian kernel of 8 mm FWHM.

Data Analysis

Data Processing

Behavioral data were analyzed using the free statistical software R (R Foundation for Statistical Computing, Vienna, Austria; www.R-project.org), SPSS 19 (IBM SPSS Statistics, Version 19), and G*Power 3 (Faul, Erdfelder, Lang, & Buchner, 2007).

The fMRI data were analyzed using the statistical parametric mapping software SPM (Wellcome Department of Imaging Neuroscience, London; www.fil.ion.ucl.ac.uk/spm/software/spm8). The first three images were excluded from the analysis, as these were acquired before the MR signal had reached its steady state.

Three participants did not perform the task properly, as indicated by the behavioral data (i.e., more than 25% errors in one or both tasks) and were accordingly excluded from further analyses.

For the remaining sample (21 participants), two onset regressors (reflecting the experimental conditions) plus associated parametric regressors (reflecting the illusion strength) were defined. Onsets were defined by the occurrence of a Müller-Lyer figure. Each appearance of a figure within a particular block was regarded as a single event. The parametric modulators coded the illusion strength of each corresponding figure. Illusion strength was coded as absolute values, that is, independently of the direction of the arrows (i.e., leftward or rightward pointing). The hemodynamic response was modeled using a canonical hemodynamic response function and its first derivative, head movement parameters were included as confounds. Effects of the first derivatives and head movements were not further investigated.

Then, different first-level contrasts were specified: First, a differential contrast comparing both experimental tasks was calculated. Second, each experimental regressor (including those reflecting parametric modulations) was compared with the implicit baseline (i.e., not explicitly modeled time periods where no event occurred). Third, a differential contrast between both parametrical regressors reflecting task related activations was calculated. These contrasts were taken to the second level, where they were subjected to one-sample t tests, using a corrected threshold of $p < .01$ at the cluster level (cluster-forming threshold $p < .001$ at voxel level). The analyses comprised contrasts between the landmark and the control task (landmark > luminance; luminance > landmark), as well as contrasts of the parametric regressors, reflecting areas showing increased neural activity with increasing illusion strength and the differential effects of illusion strength for each task. To identify visual input areas for the DCM analysis (see below), a third test was calculated reflecting the impact of both tasks (landmark + luminance task > baseline).

VOIs

On the basis of previous findings (Weidner & Fink, 2007), we included bilateral LOC and right SPC in our considerations about suitable connectivity models. In addition, we added primary visual cortex (V1) bilaterally as input regions. Consistent with Weidner and Fink (2007), the present analysis of illusion strength revealed three significant clusters of neural activity (see Results): bilateral LOC (right LOC: $x = 54, y = -70, z = -6$; left LOC: $x = -36, y = -90,$

$z = 0$) and right SPC ($x = 26, y = -62, z = 56$). Note that the former coordinates represent the peak coordinates of clusters covering temporo-occipital brain areas in both hemispheres, commonly known as LOC. Therefore, we termed both areas as LOC, well aware of the fact that the individual coordinates of the local maxima in these regions do not precisely cover congruent locations.

The three cluster peak coordinates served as centers for the VOI extraction. Additionally, two input regions bilaterally in V1 were determined (right V1: $x = 22, y = -92, z = -4$; left V1: $x = -18, y = -96, z = -16$) by masking baseline contrasts with ROIs of the right and left V1 as generated within the SPM Anatomy toolbox (Eickhoff et al., 2005). Probabilistic cytoarchitectonic maps as used in the Anatomy toolbox have been shown to largely correspond to functional localizer scans, especially in visual cortices (Wilms et al., 2010). Again, these group maxima served as centers for VOI extraction.

For every participant and each VOI, the individual activations ($p < .05$, uncorrected; cf. Eickhoff, Heim, Zilles, & Amunts, 2009) were calculated. For each VOI, a voxel was defined within a search radius of 10 mm around the corresponding group maxima. Then, the time series were extracted as the first eigenvariate of all voxel time series within a sphere (radius = 3 mm) centered on the individual peak coordinates within the search VOI. Two participants in which not all VOIs could reliably be identified were excluded, leaving a sample of 19 participants for connectivity analysis.

DCM

In the last few years, DCM (Friston et al., 2003) has successfully been used to investigate the underlying dynamics of visual processing (e.g., Cardin, Friston, & Zeki, 2011; Stephan, Marshall, Penny, Friston, & Fink, 2007; Mechelli, Price, Friston, & Ishai, 2004; Mechelli, Price, Noppeney, & Friston, 2003). Therefore, for analysis of effective connectivity, we employed DCM, as implemented in SPM8 (DCM8). To compare alternative hypotheses on the examined system as reflected by possible connectivity models,

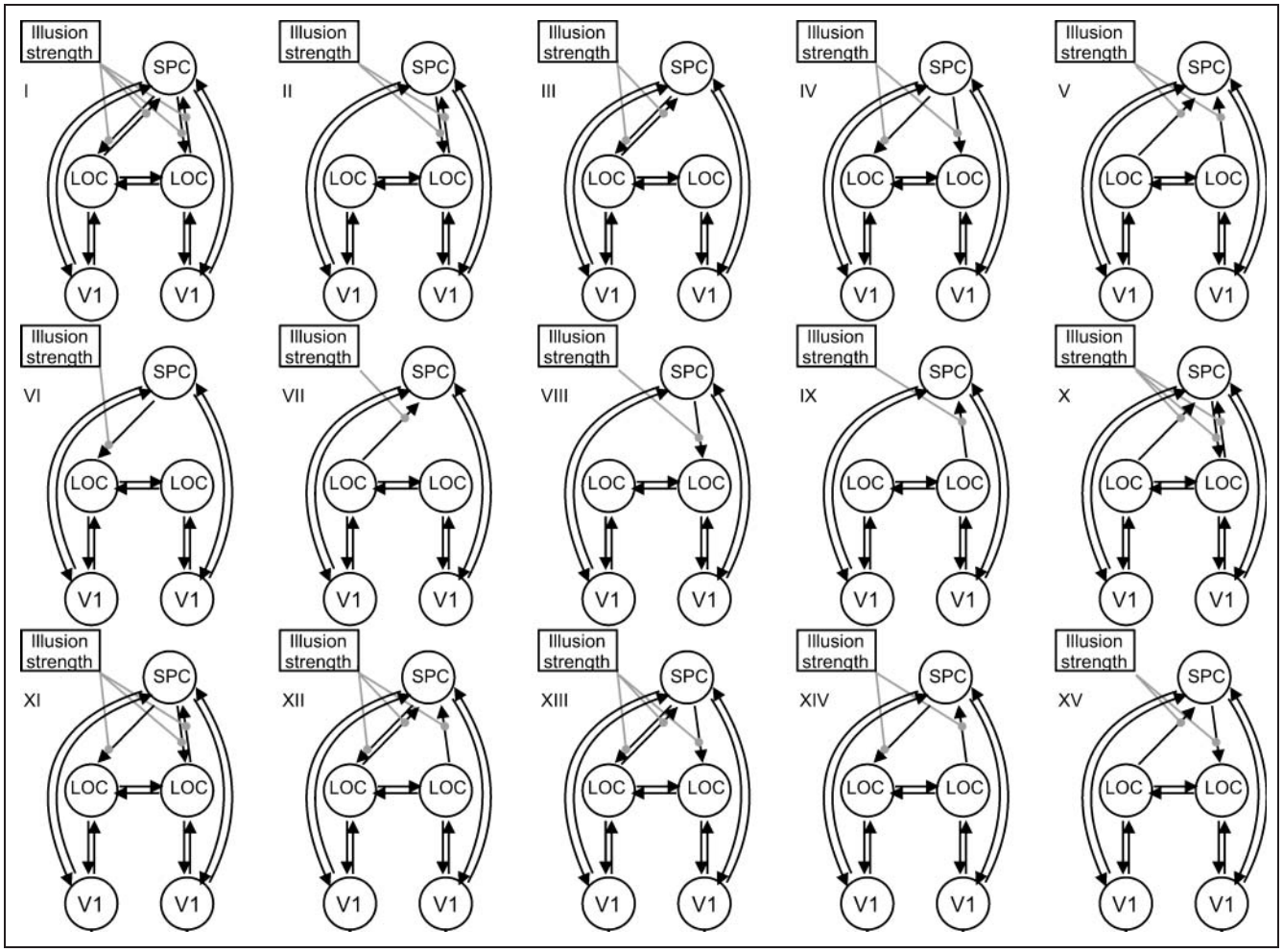

Figure 2. Outline of a possible DCM model that includes all possible connection between the chosen brain areas. The reciprocal pathways between primary visual cortex (V1) and LOC or SPC, respectively, were constant in all tested models. All other connections were systematically varied. The interaction of the SPC and LOC were of particular interest; therefore, we used "illusion strength" as modulator on these sites.

a random-effects Bayesian model selection was used (Stephan, Penny, Daunizeau, Moran, & Friston, 2009).

Using DCM, it is important to have a circumscribed and finite model space (Stephan et al., 2010). As outlined above, our DCM models consisted of bilateral V1, LOC, and right SPC. Reciprocal connections between V1 and (left/right) LOC or right SPC, respectively, as well as a reciprocal link between left and right LOC were taken as core modules for all models tested (Catani, Jones, Donato, & Ffytche, 2003; Felleman & Van Essen, 1991; Lamme & Roelfsema, 2000; Loenneker et al., 2011; Stephan et al., 2007; Zanon, Busan, Monti, Pizzolato, & Battaglini, 2009). Because LOC and SPC have been shown to be related to the processing of illusion strength (Weidner & Fink, 2007), we hypothesized that an interaction of these areas would be mandatory to explain the illusion effect. Because the neural mechanisms of ventral (LOC) and dorsal (SPC) stream interaction remain to be elucidated, we considered models that reflect all possible interactions between these areas. Overall, these considerations resulted in 15 different models, which could be categorized roughly into three groups of models (see Figure 2): models comprising only bidirectional connections (e.g., LOC ↔ SPC; Figure 2 I–III), unidirectional models (e.g., LOC → SPC, SPC → LOC; Figure 2 IV–IX) and a group of mixed models including differential connections on either side (e.g., left LOC ↔ SPC/right LOC → SPC; Figure 2 X–XV). Within every model, we modulated the connections between LOC and SPC with illusion strength to detect differences related to increasing illusion strength (under both experimental conditions).

Model Selection and Parameter Inference

To identify the most likely generative model among the 15 different DCM models, we used a random-effects Bayesian model selection procedure (Stephan et al., 2009). To test whether the coupling parameters were consistently expressed across participants, the connectivity parameters (intrinsic connections and context-dependent modulations) of the model with the highest exceedance probability were then entered into a second level analysis by means of *t* tests.

RESULTS

Behavioral Data

Pretest

The results of the angle adjustments performed to match illusion strength are shown in Figure 3. For further analyses, the two values of each condition were pooled together. To generate a 20% illusion, the mean interior angle between both wings was adjusted to $\alpha_{20} = 74.94°$ ($SD = 20.19$), whereas the angles in the 10% illusion condition on average were set to a mean of $\alpha_{10} = 127.26°$ ($SD = 15.4$). A

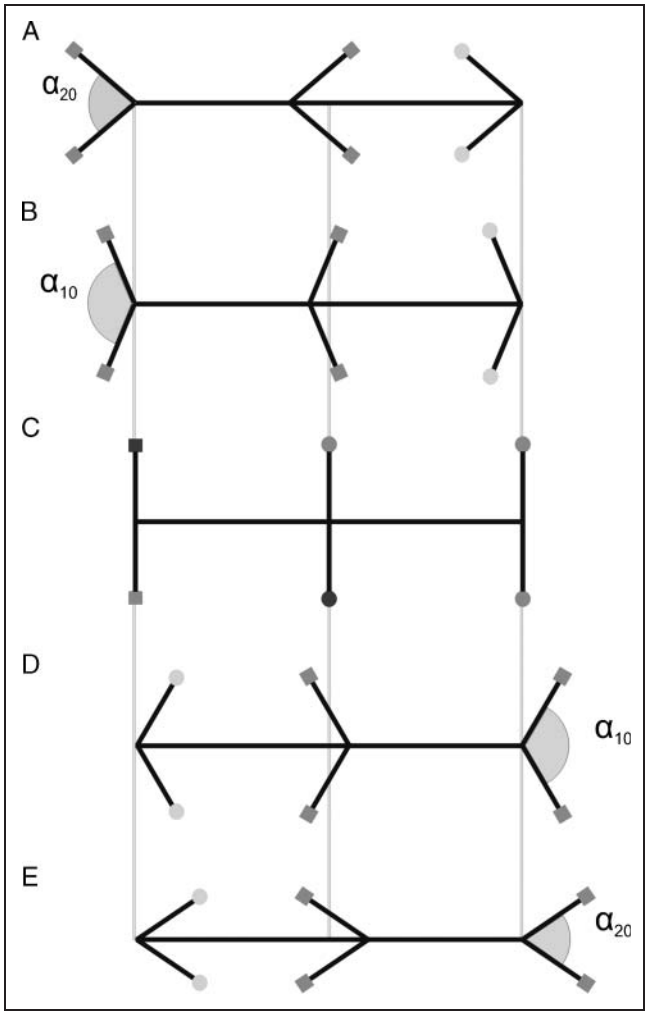

Figure 3. Examples of stimuli as presented in the fMRI experiment. The 20% illusion condition is shown in A (rightward pointing) and E (leftward pointing); B and D illustrate the 10% illusion condition. The angles (α10, α20) represent mean angles as assessed during the behavioral pretest, across the whole group, individual angle estimates differed. A neutral stimulus is shown in C, and the borders and physical middle are indicated by the bright stripes.

paired *t* test revealed a significant difference between both illusion conditions, $t(41) = -22.52$, $p < .01$, $d_z = 3.47$.

Main Experiment

Participants performed well in both tasks as indicated by an average of only 1.76% ($SD = 2.16$) trials without response across the group. In both tasks, the detection rate of the critical item did not differ [i.e., subjectively correctly bisected line: 0.89 ($SD = 0.07$) vs. coherent luminance within object: 0.86 ($SD = 0.10$), $t(20) = 1.29$, $p = .21$, $d_z = 0.27$]. At the same time, more false-positive responses were observed during the landmark task (0.15, $SD = 0.07$) relative to the luminance task (0.05, $SD = 0.06$), $t(20) = 4.64$, $p < .01$, $d_z = 1.06$. A longer mean RT for the luminance task (1.59 sec, $SD = 0.36$) as compared with the landmark task (1.31 sec, $SD = 0.21$) indicated that the

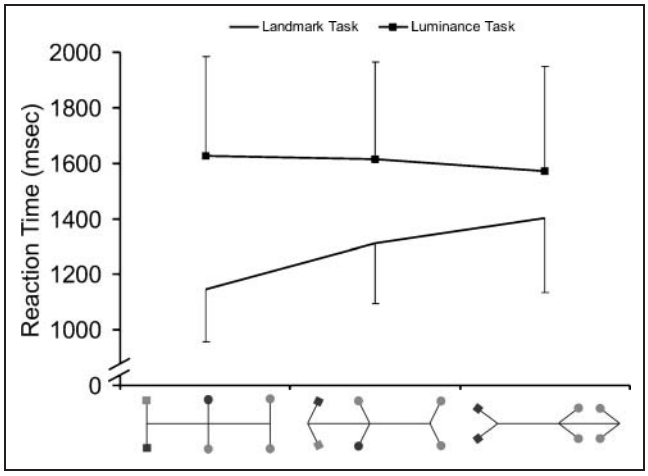

Figure 4. RTs (in msec) as observed during the main experiment. The top line represents the mean RTs across all participants during the luminance task, while the lower line shows the same information for the landmark task. The luminance task generated longer RTs. The RTs during the landmark task were differentially affected by illusion strength (i.e., stimulus configuration).

former task was more difficult ($t(20) = -5.41$, $p < .01$, $d_z = 1.14$). To further investigate this effect, a multivariate repeated MANOVA of RTs with the factors task (landmark vs. luminance) and illusion strength (strong, weak, neutral) was calculated. The MANOVA revealed a significant effect of Task, $F(1, 20) = 35.39$; $p < .01$, $\eta_p^2 = 0.64$, and Illusion Strength, $F(2, 19) = 13.07$; $p < .01$, $\eta_p^2 = 0.58$, as well as a significant Task × Figure interaction, $F(2, 19) = 24.08$; $p < .01$, $\eta_p^2 = 0.72$. In the landmark task, the participants responded faster when the neutral figure was presented and RT increased along with a stronger illusion. Additionally, a direct comparison of the single effects revealed that RTs in all three illusion conditions differed from each other (neutral vs. weak: $t(20) = -5.63, p < .01, d_z = 1.07$; neutral vs. strong: $t(20) = -7.14, p < .01, d_z = 1.22$; weak vs. strong: $t(20) = -5.63$, $p < .01$, $d_z = 1.56$). In contrast, an opposite trend was observed in the luminance task (see also Figure 4). In this condition, the fastest responses were observed for strong illusion figures. Direct comparisons within the luminance task indicated that there was solely a difference between neutral and strong

Table 1. List of Activations

Brain Region	*Side*	*Coordinates*			*Clustersize*	*T*	*p*
A. Illusion Strength							
Inferior temporal gyrus	R	54	−70	−6	1644	9.20	<.001
Middle occipital gyrus	L	−36	−90	0	1934	8.33	<.001
Superior parietal lobule	R	26	−62	56	634	5.63	<.001
B. Differential Effect of Illusion Strength (Landmark > Luminance Task)							
Superior parietal lobule	R	28	−66	50	1837	6.25	<.001
C. Landmark Task							
Supramarginal gyrus	R	66	−26	40	976	9.44	<.001
Angular gyrus	L	−54	−62	42	487	7.27	<.01
Inferior frontal gyrus	R	40	40	−10	451	6.09	<.01
Superior frontal gyrus	L	−8	42	36	1309	6.04	<.001
Inferior frontal gyrus	L	−42	38	−14	989	6.00	<.001
D. Luminance task							
Inferior parietal lobule/ superior parietal lobule/ calcarine sulcus/ fusiform gyrus*	L	−26	−54	44	24446	12.67	<.001
Precentral gyrus	L	−28	−6	48	1147	6.83	<.001
Middle frontal gyrus	R	34	0	54	794	6.03	<.001

A corrected threshold of $p < .01$ at the cluster level (cluster-forming threshold $p < .001$ at voxel level) was applied. All coordinates were defined within MNI space.

*The peak coordinate of this large cluster is located in the inferior parietal lobe, however, activation is spread along the ventral and dorsal visual streams (see Figure 5D).

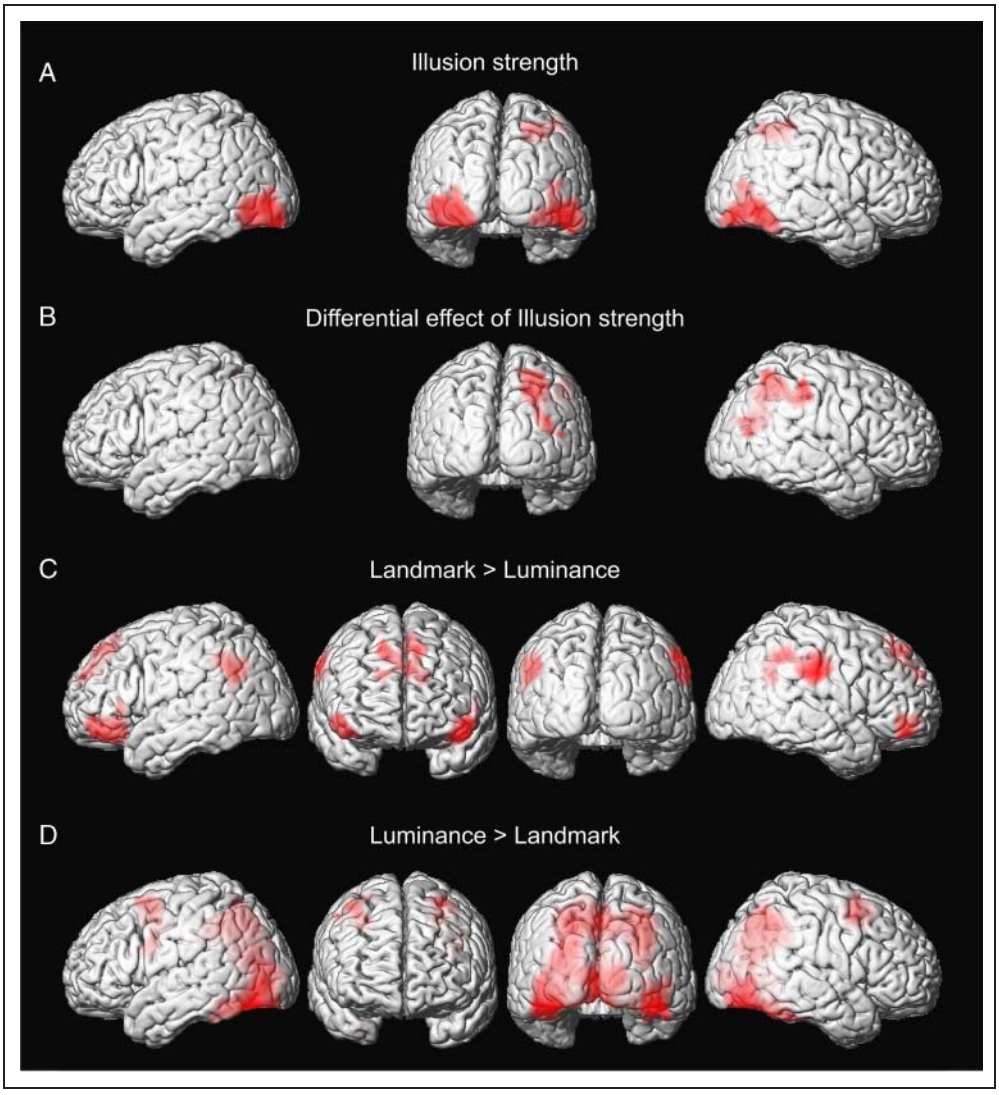

Figure 5. Surface rendering of the fMRI results obtained in the conventional SPM8 analysis. In A, the effect of the parametric modulation of illusion strength is shown, while B illustrates the differential effect of illusion strength between landmark and luminance task. Areas more activated during the landmark task when compared with the luminance task are shown in C, and D displays relative neural activations in the luminance task when compared with the landmark task. Views are shown from the left, anterior, posterior, and right direction. Because of exclusively posterior activations in A and B, no view from the anterior is presented.

illusion figures ($t(20) = 2.91, p < .01, d_z = 0.63$; all other $p > .08$).

Functional Imaging

Illusion Strength

The main effect of the Strength of the Müller-Lyer illusion was tested using parametric regressors. Consistent with previous findings (Weidner & Fink, 2007), activation positively associated with the magnitude of the illusion (independent of the task) was detected bilaterally along LOC (see Table 1A; Figure 5A), reaching from the inferior occipital gyrus to the inferior temporal gyrus. Local maxima were located in the left inferior occipital and the right inferior temporal gyrus, respectively. In addition, there was a significant activation in dorsal parietal cortex, with a peak maximum within right SPC posterior to the postcentral gyrus and in the vicinity of the intraparietal sulcus.

The latter activation in SPC was mainly driven by the parametric response of the landmark task. Testing the differential effects of illusion strength separately for each task revealed no significant increase in activation associated with illusion strength in the luminance task. To test for the specific effects of each level of the parametric regressor, we extracted the fitted response (as implemented in SPM8; cf. Henson, 2003) derived from the peak voxels of the activation clusters in LOC and SPC (as percent signal change). There was a significant increase in activity related to illusion strength and the landmark task within SPC. Whereas in the luminance condition the response in SPC remained constant irrespective of illusion strength, the response in SPC increased along with increasing illusion strength during the landmark task (see Table 1B; Figures 5B and 6). At the same time, activation in bilateral LOC similarly increased in both tasks with increasing illusion strength (see Figure 6).

Landmark and Luminance Task

Comparing the landmark to the luminance task yielded five significant clusters of activation (see Table 1C; Figure 5C). Bilateral activation was observed in inferior parietal cortex,

involving the right supramarginal gyrus as well as the right angular gyrus and furthermore the left angular gyrus. Frontal activations were observed in bilateral superior and medial frontal areas. In addition, there was bilateral activity in the anterior parts of inferior frontal cortex (pars orbitalis).

The opposite contrast (luminance > landmark task) revealed high activation within a cluster covering large parts of the ventral and dorsal visual stream, involving primary visual cortex (calcarine sulcus) extending ventrally to the fusiform gyrus and dorsally to inferior parietal cortex and SPC, also covering adjacent areas. Furthermore, a bilateral pattern of activation was revealed in the medial and the superior frontal gyrus in posterior direction slightly reaching into precentral gyrus (Table 1D; Figure 5D).

DCM

Bayesian Model Selection

A sample of 15 models, based on our predefined frame of V1, LOC, and SPC, was set up. The main focus was directed on connections between LOC and SPC. Consequently, we

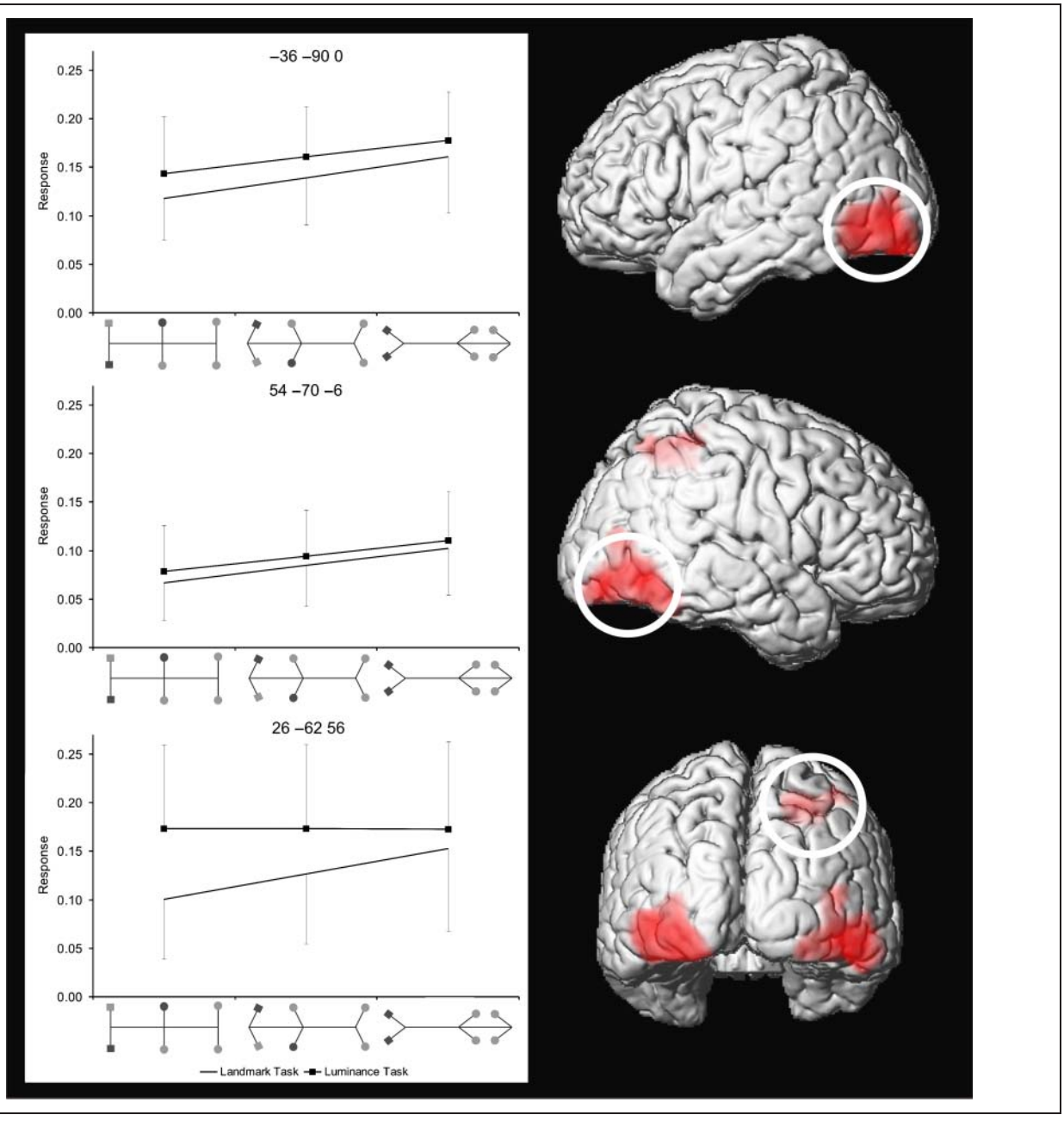

Figure 6. The graphs on the left display the fitted responses in percent signal change (within peak coordinates; brain rendering corresponds to Figure 5A: illusion strength) associated with the different figure configurations. The white circle indicates the activation locations. The upper and middle graph represent activations of the left and right LOC, respectively, and the lower graph shows activation of the right SPC. The lines with squares indicate responses during the luminance task, the bare lines indicate responses during the landmark task.

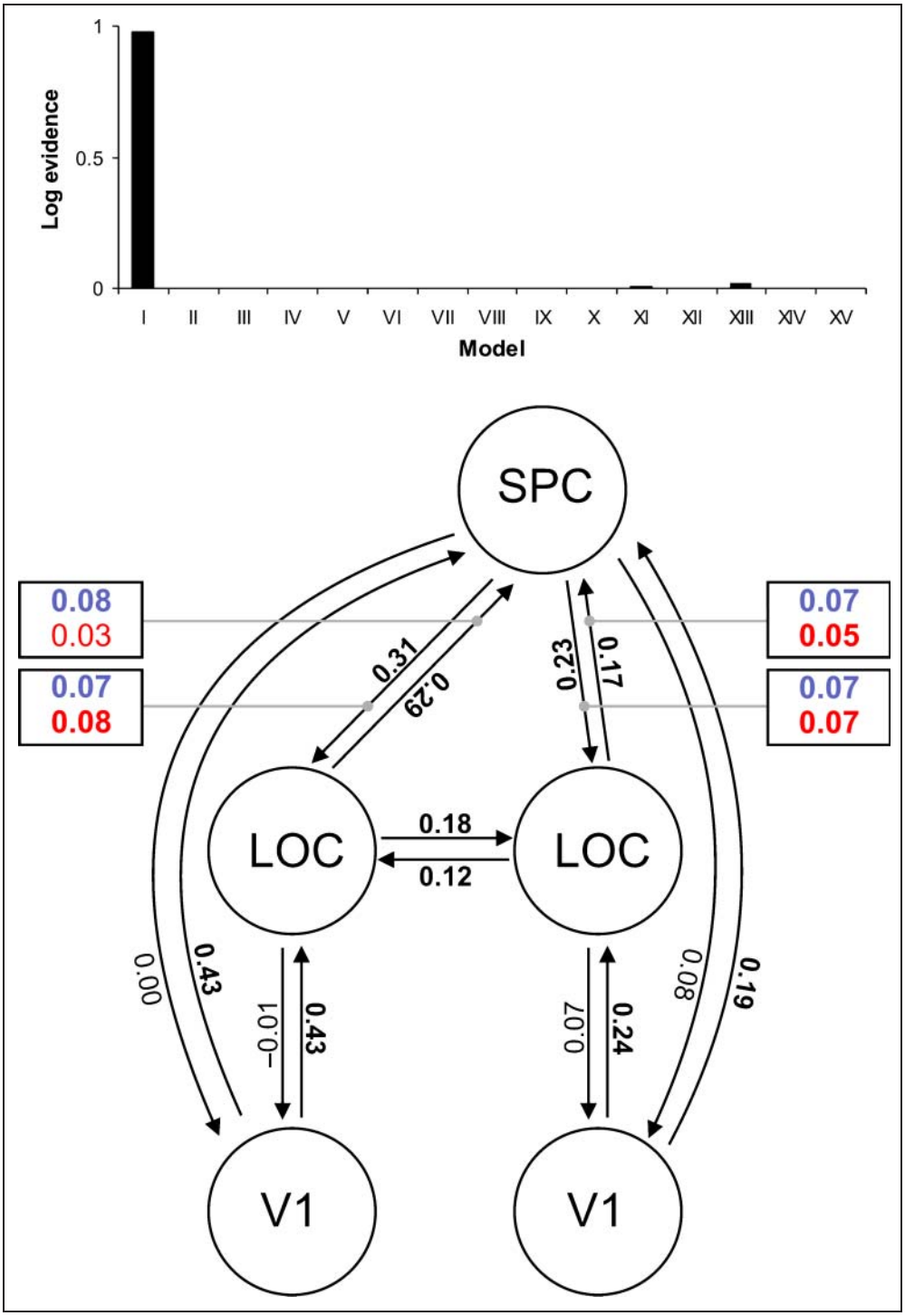

Figure 7. Top: Bars indicate the relative log evidence of each tested DCM model (model numbers correspond to those displayed in Figure 2). All models except Models I, XI, and XIII resulted in a log evidence of <.001. Bottom: Parameter values resulting from the DCM analysis displayed within the "successful" Model I. The numbers along the connections represent average parameter estimates from the tested group; significant values are highlighted in bold. The same is true for the modulatory effects where the influence of illusion strength during the landmark task is shown in blue and the influence of illusion strength during luminance task is in red. The symbols are identical to these used in Figure 2.

tested all possible connections between these structures (i.e., unidirectional, bidirectional, lateralized models; see Figure 2 and Methods for details). Furthermore, the experimental factor of illusion strength was incorporated into the models, modulating the connections between left and right LOC and SPC to reflect the influence of increasing illusion strength.

A model consisting of reciprocal connections between all given VOIs and experimental modulations on all LOC–SPC connections (see Figure 7) was found to be superior to all other models tested within a random-effects Bayesian model selection (Stephan et al., 2009) with an exceedance probability of .98. That is, the probability that this model was the most likely generative model of the observed data was 98%, whereas the likelihood of the next best model was <2% (see Figure 7).

Endogenous Connectivity and Modulatory Influence

After identifying the optimal model for the observed data, we further investigated the endogenous connectivity

and modulatory influences expressed by its parameters. The results are summarized in Figure 7 and Table 2. All feedforward connections (coupling from V1 to LOC and SPC) were significantly greater than zero. The same was true for connections between the left and right LOC as well as for connections from the left and right LOC to the right SPC and vice versa. As indicated by nonsignificant effects, feedback connections (coupling from LOC and SPC to V1) constitute a relevant part of the model but appeared to be less consistently expressed across subjects.

The interconnections between bilateral LOC and SPC were of particular interest. All connections were significantly greater than zero. Additionally, no direction-dependent effects were observed for the intrinsic connections between LOC and SPC, neither on the left nor on the right side (left: $t(18) = -0.46$, *ns*, $d_z = 0.48$; right: $t(18) = -1.86$, *ns*, $d_z = 0.43$), that is, intrinsic connectivity from LOC to SPC was not different from the reverse connections from SPC to LOC.

The bidirectional connections between LOC and SPC were differentially modulated by the landmark (Figure 7, blue numbers) and the luminance task (Figure 7, red numbers). To investigate the pattern of the modulatory effects, we calculated a repeated-measures ANOVA with the factors Task (landmark, luminance), Direction (SPC → LOC, LOC → SPC), and Side (left, right). There was no significant main effect (all $p > .46$). However, there was a significant Task × Direction interaction, $F(1, 18) = 6.73$, $p = .018$, $\eta_p^2 = 0.27$, although no other interaction reached significance (all $p > .23$). The significant interaction indicates a differential influence exerted by top–down setting on

Table 2. Parameters of the Model with the Best Fit, Including Intrinsic Connections and Modulations of the Instrinsic Connections

Intrinsic Connection	*Mean*	*SD*	*t*	*p*
Left V1 → left LOC	**0.43**	**0.15**	**12.53**	**<.001**
Right V1 → right LOC	**0.24**	**0.19**	**5.33**	**<.001**
Left LOC → left V1	−0.01	0.09	−0.53	.61
Right LOC → right V1	0.07	0.21	1.54	.14
Left V1 → SPC	**0.43**	**0.13**	**14.17**	**<.001**
Right V1 → SPC	**0.19**	**0.21**	**3.85**	**<.01**
SPC → left V1	0.00	0.19	0.02	.98
SPC → right V1	0.08	0.17	2.03	.06
Left LOC → right LOC	**0.18**	**0.22**	**3.52**	**<.01**
Right LOC → left LOC	**0.12**	**0.09**	**5.73**	**<.001**
Left LOC → SPC	**0.29**	**0.16**	**7.97**	**<.001**
Right LOC → SPC	**0.17**	**0.19**	**3.90**	**<.01**
SPC → left LOC	**0.31**	**0.15**	**8.87**	**<.001**
SPC → right LOC	**0.23**	**0.18**	**5.64**	**<.001**
Modulatory Effects by Illusion Strength (Landmark Task)				
Left LOC → SPC	**0.08**	**0.09**	**4.01**	**<.001**
Right LOC → SPC	**0.07**	**0.09**	**3.69**	**<.01**
SPC → left LOC	**0.07**	**0.11**	**2.76**	**<.05**
SPC → right LOC	**0.07**	**0.08**	**3.76**	**<.01**
Modulatory Effects by Illusion Strength (Luminance Task)				
Left LOC → SPC	0.03	0.07	1.76	.09
Right LOC → SPC	**0.05**	**0.07**	**2.99**	**<.01**
SPC → left LOC	**0.08**	**0.09**	**3.59**	**<.01**
SPC → right LOC	**0.07**	**0.08**	**4.00**	**<.001**

Significant connections are highlighted in **bold**.

connections from LOC to SPC as compared with connections from SPC to LOC.

DISCUSSION

We investigated effective connectivity within a network of brain areas involved in processing the strength of the Müller-Lyer illusion. The figures inducing the illusion were presented either in the context of a landmark task or a luminance task.

Results from the conventional fMRI analysis of regional specialization indicated that the landmark task (compared with the luminance task) activated inferior parietal cortex bilaterally, slightly stronger pronounced within the right hemisphere, which is consistent with previous experiments using similar tasks (Weidner & Fink, 2007; Fink, Marshall, Weiss, Toni, & Zilles, 2002; Fink, Marshall, Weiss, & Zilles, 2001; Fink et al., 2000). As indicated by the behavioral data, the luminance task was more demanding than the landmark task. Accordingly, activations were observed in a variety of brain regions including ventral visual areas and dorsal stream areas including superior parietal areas as well as dorsomedial and dorsolateral frontal areas.

During both tasks, the strength of the Müller-Lyer illusion was systematically altered by varying the angles of the illusion inducing arrows. Illusion strength modulated the hemodynamic response bilaterally in LOC and in right SPC, which replicates previous findings on the Müller-Lyer illusion (Weidner & Fink, 2007). To further elucidate this issue, the current study investigated effective connectivity within this network of LOC and SPC using DCM (Friston et al., 2003). A model comprising bidirectional connections between SPC and LOC was found to be superior to all other models. Following the idea of effective connectivity (Friston, 1994), this indicates that LOC and SPC exert influence upon each other.

The hemodynamic response as investigated by standard SPM analysis suggests that both regions play differential roles in generating size invariant representations. Furthermore, connectivity data as revealed by DCM indicate that both areas reciprocally modulated their activation during this process.

LOC

Increasing the strength of the Müller-Lyer illusion increases the mismatch between retinal and perceived size. Hence, more transformation is required to convert one representation into another. It has previously been demonstrated that mental size scaling is time consuming (Bennett & Warren, 2002; Bundesen & Larsen, 1975). This notion is confirmed by our behavioral data. RTs for spatial judgments increased along with increasing illusion strength. In the luminance condition, RTs were unaffected by illusion strength. However, illusory size information is coded already on a preattentive level (Busch & Müller, 2004). Accordingly, the perceived size of an object is presumably altered by the illusion, in both, the luminance as well as the landmark condition, thus implying mental size scaling. Nonetheless, because of the nonspatial nature of the luminance task, size information is not behaviorally relevant and therefore does not affect RTs.

Brain areas supporting such transformations are expected to show increased hemodynamic responses along with stimuli inducing a stronger illusion. This pattern was observed in LOC. Notably, the effect of illusion strength in LOC was without reference to specific task demands, indicating that the coding of perceived size in LOC is implemented early on, that is, at a preattentive level. Therefore, LOC is a likely candidate for executing mental size transformations (Bennett & Warren, 2002; Bundesen & Larsen, 1975).

In general, LOC is closely associated with object processing (Malach et al., 1995). Evidence derived from studies on monkeys as well as on human participants suggests that this area responds to size-invariant object properties (Sawamura, Georgieva, Vogels, Vanduffel, & Orban, 2005; Grill-Spector et al., 1999). In addition to these size-invariant representations, single-cell recordings in monkeys revealed that a large fraction of neurons in LOC are size-dependent (Lueschow, Miller, & Desimone, 1994). The joint presence of size-dependent and size-invariant neurons in LOC may indicate that this region could be involved in both generating as well as holding size invariant representations. Consistent with this notion, the current data suggest that LOC is involved in transforming initial retinal information into size invariant representations.

Whereas hemodynamic responses in LOC were found to be task-independent, connectivity analysis revealed that illusion-related transfer of information from LOC to SPC was affected by top–down settings. Although connections from LOC to SPC were generally enhanced by a stronger illusion, the spatial task further increased this influence from LOC onto SPC. Thus, these findings support the view that illusion-induced processes are, at least in part, amenable to top–down modulation (Coren & Porac, 1983, 1984; Tsal, 1984).

Right SPC

Hemodynamic responses observed in SPC also reflected illusion strength. Remarkably, this was true only for the landmark condition. During the luminance condition (i.e., without any explicit spatial task demands), the hemodynamic response pattern in SPC was virtually unaffected by the illusion. Thus, illusion coding in SPC presumably reflects postattentive processing, emerging after an initial perceived size representation has been generated.

In healthy participants, right SPC has often been shown to be involved in forming spatial judgments (Fink et al., 2000, 2001, 2002). Consequently, the data suggest that SPC requires explicit representations of (perceived) spatial

information. Our data imply that SPC utilizes perceived size representations only when these are relevant for an ongoing (spatial) task.

Interestingly, the role of SPC in spatial judgments is less clear when brain-damaged patients are considered. A recent study compared effects of neuromodulation (transcranial direct current stimulation) of parietal cortex in healthy participants and brain-damaged patients (Sparing et al., 2009). It was found that neuromodulation can have similar effects on spatial processing in patients and healthy participants, albeit those effects are more variable in patients. Additionally, it is a common finding that illusion perception is preserved following brain injuries in SPC (Olk, Harvey, Dow, & Murphy, 2001; Vallar, Daini, & Antonucci, 2000; Ro & Rafal, 1996). In contrast, illusion perception is impaired when occipital areas are affected (Vallar & Daini, 2006; Daini et al., 2002). In accordance with that, a recent study using TMS provided evidence for an involvement of lateral occipital areas in generating the Müller-Lyer illusion, whereas no clear support was found for a critical involvement of right SPC (Mancini et al., 2011). It was further suggested that SPC might be involved in integrating and updating size-invariant representations, but not in generating the illusion effect itself (Mancini et al., 2011). This assumption is strengthened by the connectivity data resulting from our DCM analysis, which indicates that SPC influences activation in LOC along with illusion strength. Hence, the SPC to LOC interactions most likely reflect processes initiated after size scaling has been performed, rather than processes generating the illusion. For instance, object representations formed and represented in LOC most likely increase in complexity along with illusion strength. Thus, further processing requires additional information from SPC, consequently the interaction between the two regions is likely to be enhanced. It has previously been reported that dorsal stream visual areas amplify and focus processing in lower-order visual areas (Seghier et al., 2000; Hupe et al., 1998). For example, Bullier suggested that information from parietal areas is used to guide processing in ventral stream visual areas via "retroinjection" (Bullier, 2001). Our data confirm the notion that dorsal areas affect activation in ventral stream areas during a visual task. However, this influence presumably reflects an evaluation rather than a generation of the object representation.

Task Difficulty and Eye Movements

Although both tasks were designed to be matched with regard to task difficulty, participants took longer to perform the luminance task. Accordingly, the luminance task may have elicited more eye movements, thus activating brain regions involved in saccade generation. These brain areas are known to reside in parietal cortex (Grefkes & Fink, 2005; Culham & Kanwisher, 2001). Therefore, an additional behavioral control experiment, identical to the fMRI experiment, was performed. Eight participants were tested and eye movements were recorded. Indeed, participants made more saccades during the luminance task as compared with the landmark task. Consequently, eye movement-related activations might be expected to be stronger in the luminance as compared with the landmark condition. Accordingly, stronger right parietal activation as observed in the landmark task is unlikely to result from differential eye movements.

Furthermore, differential saccade patterns are known to activate brain areas including frontal and supplementary eye fields (Luna et al., 1998; Petit, Clark, Ingeholm, & Haxby, 1997). Our data, however, indicate that illusion strength was associated with increased activation in right SPC as well as bilaterally in LOC. In contrast, no activation associated with illusion strength was observed in the frontal and supplementary eye fields, even when lowering the statistical threshold ($p \leq .001$, uncorrected). The data thus suggest that activations observed along with illusion strength were not triggered by differential eye movements.

Nonetheless, differential task difficulty constitutes a putative confound for the interpretation of any task comparison. The luminance task compared with the landmark task revealed a widespread activation pattern, including brain areas reflecting task difficulty. This study, however, focuses on the signal pattern related to the landmark task. There was an increase in neural activity associated with increasing illusion strength, although this was elicited basically by the easier task. A ceiling effect of activity in the luminance task also seems improbable as both tasks evoke a similar increase in LOC along with increasing illusion strength. In addition, the present findings parallel those of an earlier study on the Müller-Lyer illusion (Weidner & Fink, 2007). Although this previous study employed a much easier luminance task, the activation pattern related to illusion strength was almost identical. Moreover, the present DCM analysis indicates stronger connectivity patterns during the (easier) landmark task. On the basis of the available data, it cannot completely be ruled out that task difficulty contributes to this finding, however, it appears highly unlikely that the current findings on the Müller-Lyer illusion are solely driven by differential task difficulty.

Conclusion

In conclusion, the current study offers new insights into the mechanisms underlying illusion processing. So far, ventral and dorsal visual stream have often been regarded as functional independent entities subserving different functions (Cavina-Pratesi, Goodale, & Culham, 2007; Shmuelof & Zohary, 2005), and especially their role in illusion processing has been debated (Bruno & Franz, 2009; Bruno et al., 2008).

Our data indicate that perceiving the Müller-Lyer illusion involves a network of brain areas comprising both ventral and dorsal stream areas. However, whereas bilateral LOC is involved in size-scaling and in generating size invariant object representations, right SPC further processes these representations. Top–down settings specifically alter

connections from LOC to SPC as well as the coding of illusion information within SPC. Additionally, task-independent and illusion-related interactions from SPC to LOC reflect a facilitating processing unit, e.g., accounting for the (conscious) integration of the illusion stimuli. We therefore conclude that the generation of size invariant object representations are formed in LOC. Dorsal stream areas are involved in further utilizing these representations.

Acknowledgments

We are grateful to Petra Engels, Dorothe Krug, and Oliver Haumann for their support during data acquisition. We are also grateful to all our volunteers and our colleagues at the Institute of Neuroscience and Medicine, Research Centre Jülich.

R. W. is supported by the Deutsche Forschungsgemeinschaft (WE 4299/2-1).

Reprint requests should be sent to Thorsten Plewan, Kognitive Neurowissenschaften, Institut für Neurowissenschaften und Medizin (INM-3), Forschungszentrum Jülich, Leo-Brandt-Str. 5, 52425 Jülich, Germany, or via e-mail: t.plewan@fz-juelich.de.

REFERENCES

Ashburner, J., & Friston, K. J. (2005). Unified segmentation. *Neuroimage, 26,* 839–851.

Bennett, D. J., & Warren, W. (2002). Size scaling: Retinal or environmental frame of reference? *Perception & Psychophysics, 64,* 462–477.

Bisiach, E., Ricci, R., Lualdi, M., & Colombo, M. R. (1998). Perceptual and response bias in unilateral neglect: Two modified versions of the Milner landmark task. *Brain and Cognition, 37,* 369–386.

Brighina, F., Ricci, R., Piazza, A., Scalia, S., Giglia, G., & Fierro, B. (2003). Illusory contours and specific regions of human extrastriate cortex: Evidence from rTMS. *The European Journal of Neuroscience, 17,* 2469–2474.

Bruno, N., Bernardis, P., & Gentilucci, M. (2008). Visually guided pointing, the Müller-Lyer illusion, and the functional interpretation of the dorsal-ventral split: Conclusions from 33 independent studies. *Neuroscience and Biobehavioral Reviews, 32,* 423–437.

Bruno, N., & Franz, V. H. (2009). When is grasping affected by the Müller-Lyer illusion? A quantitative review. *Neuropsychologia, 47,* 1421–1433.

Bullier, J. (2001). Integrated model of visual processing. *Brain Research Reviews, 36,* 96–107.

Bundesen, C., & Larsen, A. (1975). Visual transformation of size. *Journal of Experimental Psychology: Human Perception and Performance, 1,* 214–220.

Busch, A., & Müller, H. J. (2004). Visual search for apparent-length targets is modulated by the Müller-Lyer illusion. *Spatial Vision, 17,* 417–441.

Cardin, V., Friston, K. J., & Zeki, S. (2011). Top–down modulations in the visual form pathway revealed with dynamic causal modeling. *Cerebral Cortex, 21,* 550–562.

Catani, M., Jones, D. K., Donato, R., & Ffytche, D. H. (2003). Occipito-temporal connections in the human brain. *Brain, 126,* 2093–2107.

Cavina-Pratesi, C., Goodale, M. A., & Culham, J. C. (2007). fMRI reveals a dissociation between grasping and perceiving the size of real 3D objects. *PLoS One, 2,* e424.

Coren, S., & Porac, C. (1983). The creation and reversal of the Müller-Lyer illusion through attentional manipulation. *Perception, 12,* 49–54.

Coren, S., & Porac, C. (1984). Structural and cognitive components in the Müller-Lyer illusion assessed via Cyclopean presentation. *Perception & Psychophysics, 35,* 313–318.

Culham, J. C., & Kanwisher, N. (2001). Neuroimaging of cognitive functions in human parietal cortex. *Current Opinion in Neurobiology, 11,* 157–163.

Daini, R., Angelelli, P., Antonucci, G., Cappa, S., & Vallar, G. (2002). Exploring the syndrome of spatial unilateral neglect through an illusion of length. *Experimental Brain Research, 144,* 224–237.

Eickhoff, S. B., Heim, S., Zilles, K., & Amunts, K. (2009). A systems perspective on the effective connectivity of overt speech production. *Philosophical Transactions, Series A, Mathematical, Physical, and Engineering Sciences, 367,* 2399–2421.

Eickhoff, S. B., Stephan, K. E., Mohlberg, H., Grefkes, C., Fink, G. R., Amunts, K., et al. (2005). A new SPM toolbox for combining probabilistic cytoarchitectonic maps and functional imaging data. *Neuroimage, 25,* 1325–1335.

Erlebacher, A., & Sekuler, R. (1969). Explanation of the Müller-Lyer illusion: Confusion theory examined. *Journal of Experimental Psychology, 80,* 462–467.

Faul, F., Erdfelder, E., Lang, A.-G., & Buchner, A. (2007). G*Power 3: A flexible statistical power analysis program for the social, behavioral, and biomedical sciences. *Behavior Research Methods, 39,* 175–191.

Felleman, D. J., & Van Essen, D. C. (1991). Distributed hierarchical processing in the primate cerebral cortex. *Cerebral Cortex, 1,* 1–47.

Fink, G. R., Marshall, J. C., Shah, N. J., Weiss, P. H., Halligan, P. W., Grosse-Ruyken, M., et al. (2000). Line bisection judgments implicate right parietal cortex and cerebellum as assessed by fMRI. *Neurology, 54,* 1324–1331.

Fink, G. R., Marshall, J. C., Weiss, P. H., Toni, I., & Zilles, K. (2002). Task instructions influence the cognitive strategies involved in line bisection judgements: Evidence from modulated neural mechanisms revealed by fMRI. *Neuropsychologia, 40,* 119–130.

Fink, G. R., Marshall, J. C., Weiss, P. H., & Zilles, K. (2001). The neural basis of vertical and horizontal line bisection judgments: An fMRI study of normal volunteers. *Neuroimage, 14,* S59–S67.

Friston, K. J. (1994). Functional and effective connectivity in neuroimaging: A synthesis. *Human Brain Mapping, 2,* 56–78.

Friston, K. J., Harrison, L., & Penny, W. D. (2003). Dynamic causal modelling. *Neuroimage, 19,* 1273–1302.

Grefkes, C., & Fink, G. R. (2005). The functional organization of the intraparietal sulcus in humans and monkeys. *Journal of Anatomy, 207,* 3–17.

Grill-Spector, K., Kushnir, T., Edelman, S., Avidan, G., Itzchak, Y., & Malach, R. (1999). Differential processing of objects under various viewing conditions in the human lateral occipital complex. *Neuron, 24,* 187–203.

Hamburger, K., & Hansen, T. (2010). Analysis of individual variations in the classical horizontal-vertical illusion. *Attention, Perception & Psychophysics, 72,* 1045–1052.

Henson, R. N. A. (2003). Analysis of fMRI timeseries: Linear time-invariant models, event-related fMRI and optimal experimental design. In R. S. J. Frackowiak (Ed.), *Human brain function* (2nd ed., pp. 793–822). Oxford: Elsevier.

Hirsch, J., DeLaPaz, R. L., Relkin, N. R., Victor, J., Kim, K., Li, T., et al. (1995). Illusory contours activate specific regions in human visual cortex: Evidence from functional magnetic

resonance imaging. *Proceedings of the National Academy of Sciences, U.S.A., 92,* 6469–6473.
Hupe, J. M., James, A. C., Payne, B. R., Lomber, S. G., Girard, P., & Bullier, J. (1998). Cortical feedback improves discrimination between figure and background by V1, V2 and V3 neurons. *Nature, 394,* 784–787.
Lamme, V. A. F., & Roelfsema, P. R. (2000). The distinct modes of vision offered by feedforward and recurrent processing. *Trends in Neuroscience, 23,* 571–579.
Loenneker, T., Klaver, P., Bucher, K., Lichtensteiger, J., Imfeld, A., & Martin, E. (2011). Microstructural development: Organizational differences of the fiber architecture between children and adults in dorsal and ventral visual streams. *Human Brain Mapping, 32,* 935–946.
Lueschow, A., Miller, E. K., & Desimone, R. (1994). Inferior temporal mechanisms for invariant object recognition. *Cerebral Cortex, 4,* 523–531.
Luna, B., Thulborn, K. R., Strojwas, M. H., McCurtain, B. J., Berman, R. A., Genovese, C. R., et al. (1998). Dorsal cortical regions subserving visually guided saccades in humans: An fMRI study. *Cerebral Cortex, 8,* 40–47.
Malach, R., Reppas, J. B., Benson, R. R., Kwong, K. K., Jiang, H., Kennedy, W. A., et al. (1995). Object-related activity revealed by functional magnetic resonance imaging in human occipital cortex. *Proceedings of the National Academy of Sciences, U.S.A., 92,* 8135–8139.
Mancini, F., Bolognini, N., Bricolo, E., & Vallar, G. (2011). Cross-modal processing in the occipito-temporal cortex: A TMS study of the Müller-Lyer illusion. *Journal of Cognitive Neuroscience, 23,* 1987–1997.
Mechelli, A., Price, C. J., Friston, K. J., & Ishai, A. (2004). Where bottom–up meets top–down: Neuronal interactions during perception and imagery. *Cerebral Cortex, 14,* 1256–1265.
Mechelli, A., Price, C. J., Noppeney, U., & Friston, K. J. (2003). A dynamic causal modeling study on category effects: Bottom–up or top–down mediation? *Journal of Cognitive Neuroscience, 15,* 925–934.
Milner, A. D., & Goodale, M. A. (1995). *The visual brain in action*. Oxford: Oxford University Press.
Müller-Lyer, F. C. (1889). Optische Urteilstäuschungen. *Archiv für Physiologie, 2,* 263–270.
Olk, B., Harvey, M., Dow, L., & Murphy, P. J. (2001). Illusion processing in hemispatial neglect. *Neuropsychologia, 39,* 611–625.
Petit, L., Clark, V. P., Ingeholm, J., & Haxby, J. V. (1997). Dissociation of saccade-related and pursuit-related activation in human frontal eye fields as revealed by fMRI. *Journal of Neurophysiology, 77,* 3386–3390.
Pressey, A., & Martin, N. S. (1990). The effects of varying fins in Müller-Lyer and Holding illusions. *Psychological Research, 52,* 46–53.
Ritzl, A., Marshall, J. C., Weiss, P. H., Zafiris, O., Shah, N. J., Zilles, K., et al. (2003). Functional anatomy and differential time courses of neural processing for explicit, inferred, and illusory contours. An event-related fMRI study. *Neuroimage, 19,* 1567–1577.
Ro, T., & Rafal, R. D. (1996). Perception of geometric illusions in hemispatial neglect. *Neuropsychologia, 34,* 973–978.
Sawamura, H., Georgieva, S., Vogels, R., Vanduffel, W., & Orban, G. A. (2005). Using functional magnetic resonance imaging to assess adaptation and size invariance of shape processing by humans and monkeys. *The Journal of Neuroscience, 25,* 4294–4306.
Seghier, M., Dojat, M., Delon-Martin, C., Rubin, C., Warnking, J., Segebarth, C., et al. (2000). Moving illusory contours activate primary visual cortex: An fMRI study. *Cerebral Cortex, 10,* 663–670.
Shmuelof, L., & Zohary, E. (2005). Dissociation between ventral and dorsal fMRI activation during object and action recognition. *Neuron, 47,* 457–470.
Sparing, R., Thimm, M., Hesse, M. D., Küst, J., Karbe, H., & Fink, G. R. (2009). Bidirectional alterations of interhemispheric parietal balance by non-invasive cortical stimulation. *Brain, 132,* 3011–3020.
Stephan, K. E., Marshall, J. C., Penny, W. D., Friston, K. J., & Fink, G. R. (2007). Interhemispheric integration of visual processing during task-driven lateralization. *The Journal of Neuroscience, 27,* 3512–3522.
Stephan, K. E., Penny, W. D., Daunizeau, J., Moran, R. J., & Friston, K. J. (2009). Bayesian model selection for group studies. *Neuroimage, 46,* 1004–1017.
Stephan, K. E., Penny, W. D., Moran, R. J., den Ouden, H. E. M., Daunizeau, J., & Friston, K. J. (2010). Ten simple rules for dynamic causal modeling. *Neuroimage, 49,* 3099–3109.
Tsal, Y. (1984). A Mueller-Lyer illusion induced by selective attention. *The Quarterly Journal of Experimental Psychology: Section A, 36,* 319–333.
Vallar, G., & Daini, R. (2006). Visual perceptual processing in unilateral spatial neglect: The case of visual illusions. In T. Vecchi & G. Bottini (Eds.), *Imagery and spatial cognition: Methods, models and cognitive assessment* (pp. 337–362). Amsterdam: John Benjamins Publishing Company.
Vallar, G., Daini, R., & Antonucci, G. (2000). Processing of illusion of length in spatial hemineglect: A study of line bisection. *Neuropsychologia, 38,* 1087–1097.
Weidner, R., Boers, F., Mathiak, K., Dammers, J., & Fink, G. R. (2010). The temporal dynamics of the Muller-Lyer illusion. *Cerebral Cortex, 20,* 1586–1595.
Weidner, R., & Fink, G. R. (2007). The neural mechanisms underlying the Müller-Lyer illusion and its interaction with visuospatial judgments. *Cerebral Cortex, 17,* 878–884.
Wilms, M., Eickhoff, S. B., Hömke, L., Rottschy, C., Kujovic, M., Amunts, K., et al. (2010). Comparison of functional and cytoarchitectonic maps of human visual areas V1, V2, V3d, V3v, and V4(v). *Neuroimage, 49,* 1171–1179.
Zanon, M., Busan, P., Monti, F., Pizzolato, G., & Battaglini, P. P. (2009). Cortical connections between dorsal and ventral visual streams in humans: Evidence by TMS/EEG co-registration. *Brain Topography, 22,* 307–317.